Journal of Solid State Chemistry 183 (2010) 1046–1054

Contents lists available at ScienceDirect

Journal of Solid State Chemistry

journal homepage: www.elsevier.com/locate/jssc

Copper(II) cyanido-bridged bimetallic nitroprusside-based complexes: Syntheses, X-ray structures, magnetic properties, ^{57}Fe Mössbauer spectroscopy and thermal studies

Zdeněk Trávníček [a,*], Radovan Herchel [a], Jiří Mikulík [a], Radek Zbořil [b]

[a] Department of Inorganic Chemistry, Faculty of Science, Palacký University, Tř. 17. listopadu 12, CZ-771 46 Olomouc, Czech Republic
[b] Department of Physical Chemistry, Faculty of Science, Palacký University, Tř. 17. listopadu 12, CZ-771 46 Olomouc, Czech Republic

ARTICLE INFO

Article history:
Received 13 November 2009
Received in revised form
23 February 2010
Accepted 1 March 2010
Available online 6 March 2010

Keywords:
Cyanido-bridged complex
Nitroprusside
Bimetallic complex
Copper spinel ferrite

ABSTRACT

Three heterobimetallic cyanido-bridged copper(II) nitroprusside-based complexes of the compositions $[Cu(tet)Fe(CN)_5NO]\cdot H_2O$ (**1**), where tet=*N,N′*-bis(3-aminopropyl)ethylenediamine, $[Cu(hto)Fe(CN)_5NO]\cdot 2H_2O$ (**2**), where hto=1,3,6,9,11,14-hexaazatricyclo[12.2.1.1^{6,9}]octadecane and $[Cu(nme)_2Fe(CN)_5NO]\cdot H_2O$ (**3**), where nme=*N*-methylethylenediamine, were synthesized and characterized by elemental analyses, ^{57}Fe Mössbauer and FTIR spectroscopies, thermal analysis, magnetic measurements and single-crystal X-ray analysis. The products of thermal degradation processes of **2** and **3** were studied by XRD, ^{57}Fe Mössbauer spectroscopy, SEM and EDS, and they were identified as mixtures of $CuFe_2O_4$ and CuO.

1. Introduction

A number of bimetallic cyanido-bridged complexes have been studied from the perspectives of the magneto-structural relationship [1], nanosized powders and molecular sieves [2]. Specifically, the compounds containing the nitroprusside $[Fe(CN)_5NO]^{2-}$ anion provide a rich variety of photo-physical properties. Combined with a suitable paramagnetic transition metal ion, the nitroprusside complexes become more interesting due to the magneto-optical correlation. The $[Fe(CN)_5NO]^{2-}$ anion is diamagnetic, but exhibits a photo induced transition to two long-live metastable states MS_1 and MS_2 upon irradiation with light in the wavelength range 350–580 nm at temperatures not higher than 160 K [3]. In addition, the incorporation of the nitroprusside anion can result in various molecular dimensionalities of the coordination compounds, which is of the great interest in supermolecular chemistry. Up to now, there exist 16 copper(II) cyanido-bridged structurally characterized complexes containing the nitroprusside anion (Cambridge Structural Database, v5.30) [4]. Most of them are dinuclear species of the type $[(L)_xCu\text{-}(\mu\text{-}NC)\text{-}Fe(CN)_4NO]\cdot yH_2O$, where *L* are usually *N*-donor bidentate ($x=2$) or tetradentate ($x=1$) ligands and number of water molecules varies between 0 and 2 [3*d*] [5]. There is only one example of a trinuclear complex: $[(CN)_4(NO)Fe\text{-}(\mu\text{-}CN)\text{-}Cu(H_2L)\text{-}(\mu\text{-}NC)\text{-}Fe(CN)_4NO]\cdot 4H_2O$, where *L*=3,10-bis(2-aminoethyl)-1,3,5,8,10,12-hexaazacyclotetradecane [6]. In four cases, the nitroprusside anion behaves as a bridging ligand forming one-dimensional (1D) molecular structures of the type $[Fe(CN)_3NO\text{-}(\mu\text{-}NC)_2\text{-}Cu(L)_x]_n\cdot ynH_2O$, where *x* is equal to 1 or 2, and *y* varies between 0 and 4 [7]. More-dimensional polymeric structures are rare, the 2D structure is observed in $[Cu_2(oxpn)Fe(CN)_5NO]$ (H_2oxpn=*N,N′*-bis(3-aminopropyl)oxamide) [8] and the 3D structure is formed only in a "pure inorganic" compound $[Cu(H_2O)Fe(CN)_5NO]\cdot H_2O$ [9].

Herein, we report the syntheses, X-ray structures, thermal and magnetic properties of three heterobimetallic cyanido-bridged Cu(II)–Fe(II) complexes, $[Cu(tet)Fe(CN)_5NO]\cdot H_2O$ (**1**), where tet=*N,N′*-bis(3-aminopropyl)ethylenediamine, $[Cu(hto)Fe(CN)_5NO]\cdot 2H_2O$ (**2**), where hto=1,3,6,9,11,14-hexaazatricyclo[12.2.1.1^{6,9}]octadecane and $[Cu(nme)_2Fe(CN)_5NO]\cdot H_2O$ (**3**), where nme=*N*-methylethylenediamine. In the case of **3**, structural and magnetic data have been re-interpreted and the obtained results compared with those published in the literature [7*e*]. The re-investigation of the magnetic properties led to different results than discussed in the cited literature.

Furthermore, the compounds **2** and **3** were tested as possible precursors for preparation of the copper spinel ferrite $CuFe_2O_4$. It has been widely used in the electronics industry due to its useful semiconducting and magnetic properties [10]. Recently, $CuFe_2O_4$ was studied also as a catalyst for removal of NO_x and diesel soot particulates [11] or catalytic performance enhancer for steam reforming of dimethyl ether [12]. In general, there are several methods to prepare spinel (nano)crystals, such as mechanical milling, hydrothermal synthesis, coprecipitation, micelle technique and others. However, the utilization of the coordination

* Corresponding author. Fax: +420 585 634 954.
E-mail address: zdenek.travnicek@upol.cz (Z. Trávníček).

0022-4596/$ - see front matter © 2010 Elsevier Inc. All rights reserved.
doi:10.1016/j.jssc.2010.03.001

compounds as starting materials for thermal degradation with the aim to prepare copper ferrite spinel structures is rare [13] based on a literature research and this work should enrich this field of material chemistry.

2. Experimental

2.1. Materials

All chemicals purchased were chemically pure, of analytical reagent grade and used without further purification.

2.2. Synthesis

Compound **1**: First, the solid dark purple crystals of $[Cu(tet)](ClO_4)_2 \cdot H_2O$ were prepared by mixing of a solution of $Cu(ClO_4)_2 \cdot 6H_2O$ (0.37 g; 1 mmol) in 15 ml of water and *N,N′*-bis(3-aminopropyl)ethylenediamine (tet; 0.17 ml; 1 mmol). $[Cu(tet)](ClO_4)_2 \cdot H_2O$ (0.45 g; 1 mmol) was dissolved in 40 ml of water, and then, a water solution (15 ml) of $Na_2[Fe(CN)_5NO] \cdot 2H_2O$ (0.30 g; 1 mmol) was added. After a week, dark purple crystals formed, which were filtered off, washed with a small amount of cold water and dried on air.

Yield: ~50%. *Anal.* Calc. for $[Cu(tet)Fe(CN)_5NO] \cdot H_2O$ ($C_{13}H_{25}CuFeN_{10}O_2$): C, 33.0; N, 29.6; H, 5.3. Found: C, 33.0; N, 29.8; H, 5.4%. (*Note*: It has been found that a number of crystal water molecules determined by X-ray analysis (1.5 H_2O) and other indirect techniques (i.e. CHN and TG/DSC analyses, 1H_2O) differs due to a length of the time interval in which the corresponding experiments were performed.) IR (cm^{-1}): 3805w, 3452s, 3312s, 3712s, 3251s, 3173sh, 2951 m, 2882 m, 2145 m, 2132s, 1914vs, 1611 m, 1597 m, 1458w, 1433w, 1290w, 1156 m, 1066 m, 1026 m, 661 m, 632sh, 509w, 408s.

Compound **2**: To a solution of $[Cu(hto)Cl]ClO_4 \cdot H_2O$ (0.47 g, 1 mmol) (prepared according to the literature [14]) in H_2O (20 ml), a water solution (10 ml) of $Na_2[Fe(CN)_5NO] \cdot 2H_2O$ (0.30 g; 1 mmol) was added. After several days, purple crystals formed. They were filtered off, washed with a small amount of cold water and dried on air. Yield: ~60%. *Anal.* Calc. for $[Cu(hto)Fe(CN)_5NO] \cdot 2H_2O$ ($C_{17}H_{30}N_{12}O_3Fe_1Cu_1$): C, 35.8; N, 29.5; H, 5.3. Found: C, 35.9; N, 29.6; H, 5.2%. IR (cm^{-1}): 3811w, 3482s, 3379s, 3226 m, 3140 m, 2885 m, 2144s, 2134s, 1916vs, 1638 m, 1469w, 1283w, 1086 m, 1066 m, 834 m, 660 m, 416s.

Compound **3**: A liquid *N*-methylethylenediamine (nme, 0.18 ml, 2 mmol) was added to a water solution (20 ml) of $Cu(ClO_4)_2 \cdot 6H_2O$ (0.37 g, 1 mmol). $Na_2[Fe(CN)_5NO] \cdot 2H_2O$ (0.30 g, 1 mmol) in 10 ml of water was added during stirring to the reaction mixture. After several days, dark purple crystals formed. They were filtered off, three-times carefully washed with a very small amount of cold water and dried on air. Yield: ~70%. *Anal.* Calc. for $[Cu(nme)_2Fe(CN)_5NO] \cdot H_2O$ ($C_{11}H_{22}N_{10}O_2Fe_1Cu_1$): C, 29.6; N, 31.4; H, 5.0. Found: C, 29.7; N, 31.2; H, 5.0%. (*Note*: It has been found that a number of crystal water molecules determined by X-ray analysis (0.5 H_2O) and other indirect techniques (i.e. CHN and TG/DSC analyses, 1H_2O) differs due to length of time interval in which the corresponding experiments were performed). IR (cm^{-1}): 3830w, 3613 m, 3435s, 3320s, 3267s, 3249s, 2952w, 2142s, 2135s, 1930vs, 1593w, 1456w, 1138w, 1090w, 1047w, 1034w, 983 m, 660 m, 412s. *Caution*: Although no problems were encountered during this work with perchlorate salts, it should be regarded as potentially explosive.

2.3. Physical measurements

Elemental analyses (C, H, N) were performed on a Fisons EA1108 CHN analyzer. IR spectra (400–4000 cm^{-1}) were obtained by a ThermoNicolet NEXUS 670 FT-IR spectrometer using KBr pellets. The transmission ^{57}Fe Mössbauer spectra were collected using a Mössbauer spectrometer in a constant acceleration mode with a ^{57}Co(Rh) source and all presented data are relative to natural α-iron foil. The measurements were carried out at room temperature and at 25 K using a closed-helium-cycle cryostat. Variable temperature and variable magnetic field magnetization measurements on polycrystalline samples were carried out with an MPMS XL-7 Quantum Design SQUID magnetometer. The experimental data were corrected for the diamagnetism of the constituent atoms by using Pascal's constants [15], and for the diamagnetism of the sample holder. Also, the temperature independent paramagnetism (TIP) parameter $\alpha_{TIP} = 0.75 \times 10^{-9}\ m^3\ mol^{-1}$ for Cu(II) was used during the fitting procedures. Simultaneous thermogravimetric (TG) and differential thermal (DTA) analyses were performed using an Exstar TG/DTA 6200 thermal analyzer (Seiko Instruments Inc.) in a ceramic crucible in dynamic air atmosphere (150 mL min^{-1}) from laboratory temperature to 1000 °C (gradient 5 °C min^{-1}). The thermal degradation products were prepared as follows: the complex compounds were heated in the oven with the temperature gradient of 5 °C min^{-1}. After reaching 850 °C, the temperature in the oven was stabilized for the next 4 h. Scanning electron microscopy (SEM) images were obtained on Hitachi SU-6600 (FEG, SE image resolution 1.2 nm at 30 kV). The pictures were collected with high voltage of 5 kV at a working distance of 10 mm. The sample material was fixed on carbon conductive discs. No coating method was used. Energy dispersive X-ray spectra (EDS) were collected by a Si(Li) X-ray detector together with NORAN System 7 (Thermo Scientific) mounted on SEM.

2.4. X-ray data collection and refinement

X-ray experiments were carried out on a four circle κ-axis Xcalibur™2 diffractometer equipped with a CCD detector Sapphire2 using graphite monochromated Mo–Kα radiation, (Oxford Diffraction, UK). The CrysAlis program package (version 1.171.32.11, Oxford Diffraction) was used for data collection and reduction [16]. The structures of the complexes were solved by the direct methods using SHELXS-97 program [17]. All non-hydrogen atoms of the compounds **1–3** were refined anisotropically by the full-matrix least-squares procedure [SHELXL-97] [17]. As for **1**, all H-atoms, except for those of both water molecules, were found from Fourier difference maps and refined using a riding model (AFIX 13, AFIX 23 and AFIX 137 instructions were used). Hydrogens belonging to the crystal water molecules were not involved into calculation. In the case of **2** and **3**, all H-atoms were found from Fourier difference maps and refined using a riding model, except for those of crystal water molecules which were refined freely with fixed U_{eq} parameters. As for **3**, a part of the nme ligand was refined as disordered over two positions with the occupancy factor of 53% for the first component and 47% for the second one. Additional calculations were performed using the DIAMOND program [18]. Crystal data and structure refinement of **1–3** are summarized in Table 1 while selected interatomic parameters are given in Table 2.

3. Results and discussion

3.1. Infrared spectroscopy

Infrared spectroscopy confirmed the presence of lattice water and amino-ligands in the compounds **1–3** as proved by observation of the ν(O–H) and ν(N–H) vibrations in the 3600–3200 cm^{-1}

Table 1
Crystal data and structure refinements for **1**–**3**.

Data	**1**	**2**	**3**
Empirical formula	$C_{52}H_{88}Cu_4Fe_4N_{40}O_{10}$	$C_{17}H_{30}CuFeN_{12}O_3$	$C_{22}H_{38}Cu_2Fe_2N_{20}O_3$
Formula weight	1911.18	569.92	869.50
Collection T (K)	100(2)	100(2)	100(2)
λ (Å)	0.71073	0.71073	0.71073
Crystal system	Orthorhombic	Monoclinic	Triclinic
Space group	$Pc\ a2_1$	$P2_1/n1$	$P-1$
a (Å)	10.1644(9)	10.2389(2)	7.52830(10)
b (Å)	13.009(3)	12.5798(2)	9.42600(10)
c (Å)	15.229(3)	19.0070(3)	13.8474(2)
a (deg.)	90	90	86.3768(13)
β (deg.)	90	97.0098(17)	81.0979(14)
γ (deg.)	90	90	71.3285(15)
V (Å^3)	2013.7(6)	2429.86(7)	919.61(2)
Z	1	4	1
D_{calc} (g cm^{-3})	1.576	1.558	1.570
μ (mm^{-1})	1.810	1.517	1.969
Min/max trans.	0.6604/0.5700	0.6589/0.6187	0.6942/0.5064
hkl ranges	$-12 \le h \le 12$ $-15 \le k \le 15$ $-18 \le l \le 15$	$-12 \le h \le 12$ $-10 \le k \le 14$ $-22 \le l \le 22$	$-8 \le h \le 8$ $-11 \le k \le 10$ $-15 \le l \le 16$
Total reflections	12618	14649	6244
Unique reflections	2961	4277	3221
R (int)	0.0929	0.0103	0.0097
Parameters/restraints	278/1	319/4	250/2
R_1 (all data)	0.0531	0.0532	0.0259
R_1 ($I > 2\sigma(I)$)	0.0512	0.0515	0.0234
wR_2 (all data)	0.1277	0.1165	0.0832
wR_2 ($I > 2\sigma(I)$)	0.1267	0.1159	0.0742
Max/min residual (e Å^{-3})	0.728/−0.493	1.174/−0.738	0.724/−0.423
G.O.F.	1.116	1.326	1.249

Table 2
Selected bond lengths (Å) and angles (°) of **1**-**3**.

Compound **1**[a]		Compound **2**		Compound **3**[b]	
Fe1–N6	1.651(6)	Fe1–N1	1.665(4)	Fe1–N6	1.6632(18)
Fe1–C5	1.931(8)	Fe1–C3	1.929(4)	Fe1–C4	1.939(2)
Fe1–C2	1.939(8)	Fe1–C5	1.932(4)	Fe1–C2	1.939(2)
Fe1–C4	1.940(7)	Fe1–C6	1.937(4)	Fe1–C3	1.941(2)
Fe1–C1	1.942(8)	Fe1–C2	1.938(5)	Fe1–C5	1.947(2)
Fe1–C3	1.944(7)	Fe1–C4	1.949(4)	Fe1–C1	1.947(2)
Cu1–N5♯1	2.361(8)	Cu1–N10	1.986(3)	Cu1–N9	2.0302(19)
Cu1–N7	2.024(6)	Cu1–N7	2.009(4)	Cu1–N10	2.0535(18)
Cu1–N10	2.039(6)	Cu1–N8	2.045(3)	Cu1–N2	2.4503(19)
Cu1–N8	2.049(6)	Cu1–N9	2.060(3)	Cu2–N8	2.0112(19)
Cu1–N9A	2.114(13)	Cu1–N5	2.259(4)	Cu2–N7	2.047(2)
Cu1–N9	1.962(17)			Cu2–N5	2.565(2)
Cu1–N2	2.5946(84)				
O1–N6	1.134(9)	O1–N1	1.131(5)	O1–N6	1.139(2)
N6–Fe1–C2	177.1(3)	N1–Fe1–C4	178.32(17)	N6–Fe1–C5	174.73(9)
C5–Fe1–C1	170.7(4)	C3–Fe1–C5	170.95(17)	C4–Fe1–C2	170.51(9)
C4–Fe1–C3	170.3(3)	C3–Fe1–C5	169.20(19)	C3–Fe1–C1	168.55(9)
O1–N6–Fe1	176.9(7)	O1–N1–Fe1	177.5(4)	O1–N6–Fe1	174.29(17)
N7–Cu1–N9	166.6(5)	N10–Cu1–N7	168.21(16)	N9–Cu1–N9♯1	180.00(10)
N7–Cu1–N9A	174.1(4)	N8–Cu1–N9	168.23(15)	N10–Cu1–N10♯1	180.0
N10–Cu1–N8	173.0(3)			N2–Cu1–N2♯1	180.0
N2–Cu1–N5♯1	177.7(3)			N8–Cu2–N8♯1	180.0
				N7–Cu2–N7♯2	180.0
				N5–Cu2–N5♯2	180.0
Fe1–C2–N2	177.2(7)	Fe1–C5–N5	176.6(4)	Fe1–C2–N2	176.95(19)
Cu1–N2–C2	138.3(7)	Cu1–N5–C5	156.3(4)	Cu1–N2–C2	139.48(17)
Fe1–C5–N5	179.3(8)			Fe1–C5–N5	175.2(2)
Cu1♯2–N5–C5	161.8(8)			Cu2–N5–C5	126.54(18)

Symmetry transformations used to generate equivalent atoms:

[a] ♯1: $-x+3/2, y, z-1/2$; ♯2: $-x+3/2, y, z+1/2$.
[b] ♯1: $-x+1, -y+2, -z$; ♯2: $-x+1, -y+1, -z+1$.

region. Characteristic vibrations of the nitroprusside anion $[Fe(CN)_5NO]^{2-}$ were also observed for all compounds. The two absorption peaks in 2132–2135 cm^{-1} and 2142–2145 cm^{-1} regions can be assigned to the terminal, and bridging cyanido groups, respectively [19]. The strong absorption peaks in the 1914–1930 cm^{-1} region for **1**–**3** obviously correspond to the ν(N=O) vibration [20].

3.2. X-ray crystallography

The single crystal X-ray analysis of **1** revealed a cyanido-bridged *zig-zag* chain structure in which iron(II) is six-coordinated by one nitrogen atom of the nitrosyl group and five carbon atoms of the cyanido ligands, while copper(II) is six-fold coordinated by four nitrogen atoms of the *tet* ligand in the equatorial plane and two nitrogen atoms from different bridging cyanido groups in apical positions. The in-plane Cu–N bond lengths range from 1.962(17) Å [for Cu(1)–N(9)] to 2.114(13) Å [for Cu(1)–N(9A)], while the apical Cu–N distances are significantly longer with the Cu–N distances of 2.361(8) Å [for Cu(1)–N(5)] and 2.5946(84) Å [for Cu(1)–N(2)], resulting in the elongated tetragonal bipyramide symmetry of a $\{CuN_6\}$ chromophore. The nitroprusside anions are coordinated in such a way that the copper(II) ions are bridged through the cyanido groups in a *cis* fashion and the Fe–C distance in the bridged CN groups is shortened [Fe(1)−C(5)=1.931(8) Å, Fe(1)−(C2)=1.939(8) Å] in comparison with the remaining and free CN groups in which the average distance is 1.942 Å. For comparison, average values of the Fe–C and Fe–N bond lengths, as determined by the analysis of 69 complexes involving the $Fe(CN)_5NO$ motif and deposited within the Crystallographic Structural Database (CSD version 5.30, Update May 2009) [4], have been found to be 1.937 Å, and 1.653 Å, respectively. On the other hand, the average Cu–N distance in the $(CN)_4(NO)Fe$-(μ-CN)-CuN_5 motif, as determined from 17 complexes, is 2.172 Å. The Cu…Fe separations alternate in the cyanido-bridged *zig-zag* chain structure of **1** and have been found to be 5.3761(15), and 5.2727(13) Å, respectively, while the average value found from 19 compounds involving the $(CN)_4(NO)Fe$-(μ-CN)-Cu motif equals 5.122 Å. The crystal structure of **1** is stabilized by a network of the N–H…O and N–H…N hydrogen bonds. A part of the crystal structure of **1** is shown in Fig. 1, while selected bond lengths and angles are listed in Table 2.

The asymmetric unit of the crystal structure of **2** comprises the binuclear unit in which the copper(II) cation has a penta-fold coordination, consisting of four nitrogen atoms of the hto ligand forming the equatorial plane, while the nitrogen atom of the cyanido group of the nitroprusside anion is coordinated in the apical position—Fig. 2(top). The Cu–N bond lengths within

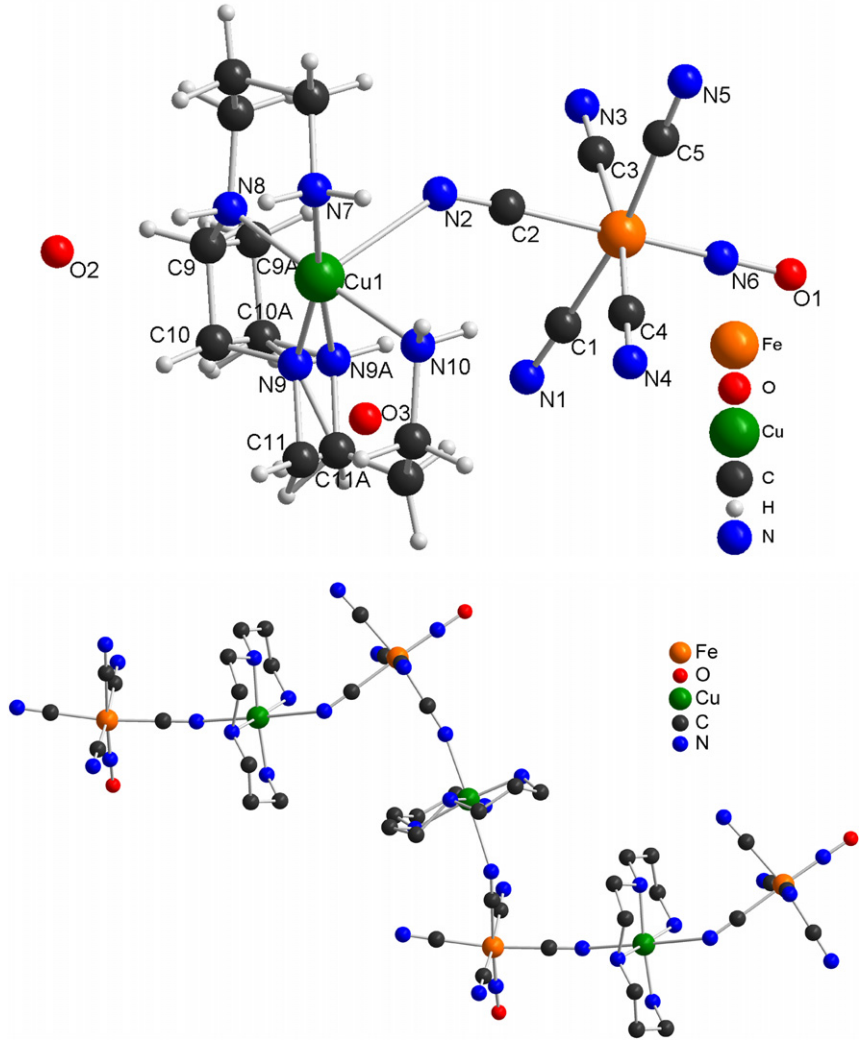

Fig. 1. Top: the asymetric unit of $[Cu(tet)Fe(CN)_5NO] \cdot 1.5H_2O$ (**1**) showing the disordered tet ligand. Bottom: a part of the crystal structure showing the zig-zag chain motif. The water molecules and hydrogen atoms are omitted for the sake of clarity.

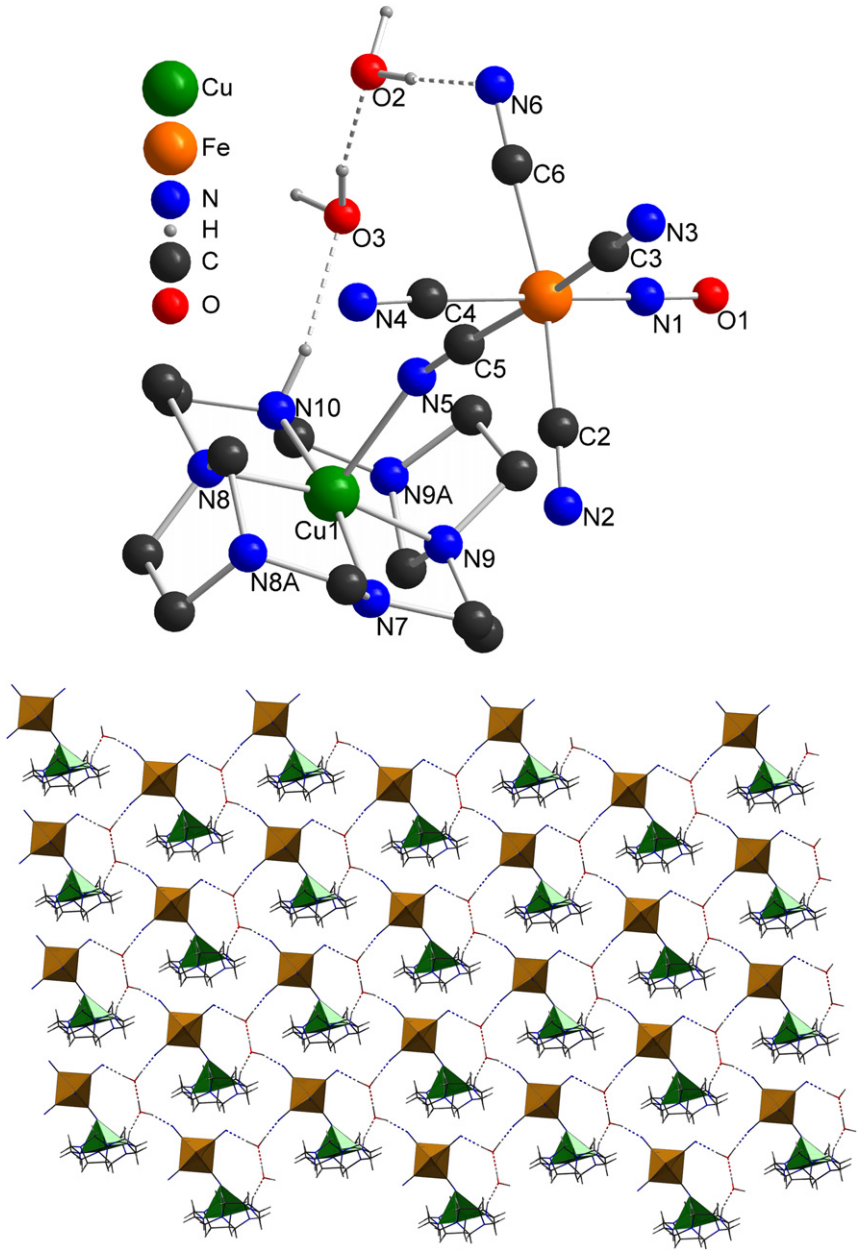

Fig. 2. Top: the molecular structure of $[Cu(hto)Fe(CN)_5NO]\cdot 2H_2O$ (**2**). Only the hydrogen atoms incorporated into the hydrogen bonds (dashed lines) are displayed for the sake of clarity. Bottom: a part of the crystal structure showing the hydrogen bonds (dashed lines), a view down along the b axis.

the $[Cu(hto)]^{2+}$ core are similar and range from 1.986(3) to 2.060(3) Å. The apical Cu–N distance is considerably longer with the Cu(1)–N(5) bond length value of 2.259(4) Å. The Fe–C distances in the nitroprusside anion for monodentate coordinated cyanido ligands vary from 1.929(4) to 1.949(4) Å, while the same distance associated with a bridging CN group is 1.932(4) Å. The Cu…Fe separations have been found to be 5.2035(8) Å within the crystal structure of **2**. The crystal structure contains two molecules of crystal water. The first water molecule (containing the O2 atom) forms hydrogen bonds among the different nitroprusside anions, while the second one (containing the O3 atom) is bonded to the other cyanido group of nitroprusside anions and also to the N–H atoms of the hto ligand-Fig. 2(bottom). Thus, the crystal structure of **2** is stabilized by a network of the O–H…O, O–H…N, N–H…O N–H…N hydrogen bonds, whose parameters are summarized in Table 3.

The X-ray structure of $[Cu(nme)_2Fe(CN)_5NO]\cdot H_2O$ **3** has been already determined at 293 K and published [7*e*], with the following crystal data and refinement parameters: $T=293$ K, $R(\text{int})=0.021$. $a=7.6429(10)$, $b=9.4444(12)$, $c=13.9990(18)$, $\alpha=85.602(2)$, $\beta=81.544(2)$, $\gamma=71.681(2)$. $F(0\,0\,0)=458$. $R1=0.0352$. $wR2=0.0862$ (for 3051 independent reflections). Max/min residual ($e\,Å^{-3}$)=0.920/−0.607. Owing to the fact that we have decided to re-interpret the magnetic data of this complex, we have performed structural re-investigation of $[Cu(nme)_2Fe(CN)_5NO]\cdot 0.5H_2O$ (**3**) at 100 K with the aim to support the interpretation of magnetic data. The crystal data and structure refinement of **3** are given in Table 1, while selected interatomic parameters are listed in Table 2. The Cu…Fe separations have been found to be 4.9925(3) and 5.1684(3) Å within the crystal structure of one-dimensional chain complex **3**. A part of the crystal structure of **3**, showing the 1D chain motive, is depicted in Fig. A1 (see Appendix A, Supplementary Material).

Table 3
Hydrogen bond lengths (Å) and angles (deg.) for **1**–**3**.

D–H···A	D–H	H···A	D···A	D–H···A
Compound **1**[a]				
N9–H9E···O3	0.93	2.21	2.93(2)	132.9
N9A–H9AA···N2	0.93	2.60	3.061(17)	111.2
N7–H7C···N1♯3	0.92	2.48	3.324(14)	152.0
N7–H7D···N4♯4	0.92	2.25	3.120(9)	157.2
N8–H8C···O2	0.93	2.28	2.814(13)	115.9
N10–H10A···N4	0.92	2.57	3.397(10)	149.1
N10–H10B···N4♯4	0.92	2.36	3.261(9)	166.7
Compound **2**[b]				
N10–H10C···O3	0.93	1.95	2.849(5)	160.9
O2–H2W···N6	0.90(3)	2.05(3)	2.948(5)	173(5)
O3–H3W···O2	0.92(3)	1.85(3)	2.751(5)	167(5)
N7–H7C···N3♯1	0.93	2.34	3.079(6)	136.0
O2–H V···N2♯2	0.91(3)	1.93(3)	2.818(5)	166(5)
Compound **3**[c]				
N9-H9D···N1	0.92	2.68	3.421(3)	137.7
N7-H7C···O2	0.77(4)	2.42(4)	2.855(5)	117(3)
N8-H8A···N4♯3	0.92	2.15	3.008(3)	154.6
N9-H9E···N3♯4	0.92	2.28	3.095(3)	147.7
N10-H10C···N3♯5	0.93	2.23	3.097(3)	155.6
O2-H2W···N3♯2	1.01(3)	2.49(4)	3.429(5)	155(5)
O2-H2V···N1♯6	0.99(3)	1.90(3)	2.881(4)	174(6)
N7-H7C···N4♯2	0.77(4)	2.57(4)	3.293(3)	158(4)

Symmetry transformations used to generate equivalent atoms:

[a] ♯3: $x+1, y, z$; ♯4: $x+1/2, -y+2, z$.

[b] ♯1: $x+1, y, z$; ♯2: $x-1/2, -y+3/2, z-1/2$.

[c] ♯2: $-x+1, -y+1, -z+1$; ♯3: $-x+2, -y+1, -z+1$; ♯4: $x, y+1, z$; ♯5: $x-1, y+1, z$; ♯6: $-x+1, -y+2, -z+1$.

3.3. Magnetic properties

The compounds **1** and **3** form infinite one-dimensional (1D) chains, in which the paramagnetic Cu(II) centers are bridged through the diamagnetic nitroprusside anions; their magnetic data scaled per one Cu(II) ion are depicted in Fig. 3 and Fig. A2 (see Appendix A, Supplementary Material). The effective magnetic moment at room temperature is 1.86 and 1.91 μ_B, for **1**, and **3**, respectively. These values are close to the expected value for non-interacting copper(II) complexes with $S=1/2$ and $g>2.0$ due to the orbital momentum contribution [21]. Upon cooling, the effective magnetic moments stay almost constant to about 20 K, and then, start to decrease gradually to reach 1.71 μ_B at 2 K for both compounds. The mean susceptibility of **1** and **3** can be fitted to the Curie–Weiss law (in SI units)

$$\chi_{mol} = \frac{N_A \mu_0 \mu_B^2 S(S+1)}{3k} \frac{g^2}{T-\Theta} \quad (1)$$

using the following parameters $g=2.13$, $\Theta=-1.34$ K and $g=2.20$ and $\Theta=-1.33$ K, respectively. Based on these facts, the antiferromagnetic exchange between the Cu(II) ions is present both in **1** and **3**. The isothermal magnetizations measured at $T=2$ K saturate at $M_{mol}/(N_A\mu_B)=1.02$ for **1** and 1.07 for **3**. These values are close to the expected saturation limit of $M_{mol}/(N_A\mu_B)=1.0$ for $g=2.0$ and $S=1/2$. In order to quantitatively evaluate the magnetic exchange among paramagnetic copper(II) ions, the following spin Hamiltonian for the uniformly coupled one-dimensional infinite chain should be applied

$$\hat{H} = -J\sum_{i=1}^{\infty} \mathbf{S}_i \cdot \mathbf{S}_{i+1} + \mu_B \sum_{i=1}^{\infty} \mathbf{B} \cdot \mathbf{g}_i \cdot \mathbf{S}_i \quad (2)$$

Unfortunately, the analytical expression for the molar susceptibility cannot be derived, but a numerically derived expression by Johnston et al. can be used with a high accuracy [22]. The best-fit

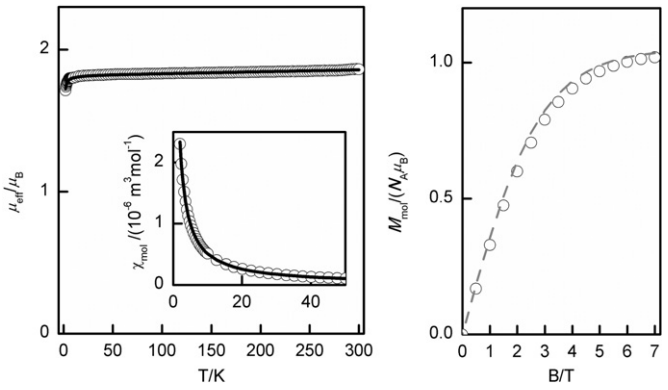

Fig. 3. Magnetic data for **1**. Left: temperature dependence of the effective magnetic moment (calculated from the temperature dependence of magnetization at $B=1$ T). Inset: temperature dependence of the molar susceptibility. Empty circles: experimental points. Full line: the best fit to the experimental data calculated using Eq. (2) with $J=-0.28\ cm^{-1}$ and $g=2.10$. Right: field dependence of magnetization at $T=2.0$ K. Empty circles: experimental points. Dashed line: the Brillouin law for the isolated copper(II) ion.

parameters to the magnetic susceptibility, which were calculated from the temperature dependence of the magnetization measured at 1 T, resulted in the following parameters: $J=-0.28\ cm^{-1}$, $g=2.10$ for **1** and $J=-0.43\ cm^{-1}$, $g=2.16$ for **3**—Figs. 3 and A2. The small value of the isotropic exchange can be readily explained by a long distance superexchange pathway between the copper ions mediated by the diamagnetic nitroprusside anion and is comparable with recently published values $J=-0.12\ cm^{-1}$ [7*a*], $J=-1.06\ cm^{-1}$ [7*c*] and $J=-1.7\ cm^{-1}$ [7*b*]. Also, the Brillouin functions, calculated at $T=2$ K for $S=1/2$ using the resulted *g*-factors, are slightly above the experimental data, which confirms antiferromagnetic nature of the isotropic exchange among the paramagnetic centers. The comparison of the previously published magnetic data for $[Cu(nme)_2Fe(CN)_5NO]\cdot H_2O$ with those found for (**3**) in this work is depicted in Fig. A4 (see Appendix A, Supplementary Material), and it clearly shows that the authors did not apply diamagnetic corrections and the temperature-independent paramagnetism, which resulted in misinterpretation of the magnetic exchange. (*Note*: A number of crystal water molecules in **3** as determined by X-ray analysis (0.5 H_2O) and other indirect techniques (i.e. CHN and TG/DSC analyses, $1H_2O$) differs probably due to time interval between the corresponding experiments.)

Moreover, the advanced theoretical approach was used, in which the both experimental datasets (the magnetizations vs. temperature and vs. magnetic field) were treated simultaneously. There is no numerical or analytical formula for the isothermal magnetization of the infinite uniform 1D chain for non-zero temperature, so we treated the problem as follows: the spin Hamiltonian for the seventeen-nuclear closed ring was postulated as

$$\hat{H} = -J\left\{\sum_{i=1}^{16} \mathbf{S}_i \cdot \mathbf{S}_{i+1} + (\mathbf{S}_{17} \cdot \mathbf{S}_1)\right\} + \mu_B \sum_{i=1}^{17} \mathbf{B} \cdot \mathbf{g}_i \cdot \mathbf{S}_i \quad (3)$$

in order to mimic the infinite chain properties. Such a procedure is generally used for the infinite chains to calculate their physical properties, e.g. susceptibility or heat capacity. To examine the limits for this model, the zero-field susceptibilities, hence the effective magnetic moments, were calculated using Johnston's equation [22] and finite-size ring model (Eq. (3)) at the lowest experimental temperature $T=2$ K (the plot comparing these two calculations is given in Supplementary material, Appendix A, Fig. A5). It was found that both models provide similar results for varying $|J|$ up to 8 cm^{-1}. Below this value, the discrepancy is less than 0.01 μ_B, which is much smaller than the experimental error.

The 17 centers with $S_i=1/2$ result in 131 072 magnetic states. In order to reduce the dimensions of the matrices to be diagonalized, the coupled basis set was chosen labeled as $|\alpha SM_S\rangle$, where α stands for the intermediate quantum numbers denoting the coupling path. The final interaction matrices were calculated using irreducible tensor operators technique [23]. Having only the isotropic exchange in play and also all local g-factors equal, the matrices can be factorized according to the final spin S and it is possible to treat only zero-field magnetic states $|\alpha S\rangle$. The largest dimension of the sub-matrix is 7072 for $S=3/2$ (see Table A1; in Appendix A, Supplementary material). As a result, the magnetic levels can be easily calculated as $\varepsilon_j(\alpha SM_S)=\varepsilon_{i,0}(\alpha S)+\mu_B g M_S B$, where $\varepsilon_{i,0}(\alpha S)$ are zero-field energy levels. Finally, the formula for the molar magnetization for any temperature and magnetic field can be applied as

$$M_{\mathrm{mol}} = N_A \mu_B g \frac{\sum_j M_S \exp[-\varepsilon_j(\alpha SM_S)/kT]}{\sum_j \exp[-\varepsilon_j(\alpha SM_S)/kT]} \quad (4)$$

The best fit for **1** was obtained using $J=-0.23\,\mathrm{cm}^{-1}$, $g=2.10$ (Fig. 4) and for **3** using $J=-0.38\,\mathrm{cm}^{-1}$, $g=2.16$ (Fig. A3). The calculated g-parameters from both fits are practically identical. On the contrary, the J constants differ by more than 10%. The reason for this discrepancy lies in the large field applied for measuring the temperature dependence of magnetization. The formula by Johnston et al. [22] was derived upon presumption that the magnetic field is close to zero ($B\to 0$). The effect of the magnetic field on the effective magnetic moment is demonstrated in Fig. A6 (see Appendix A, Supplementary Material). Based on these facts, the second set of the fitted parameters is more reliable.

The magnetic data of the binuclear complex **2** are presented in Fig. 5. The room temperature value of the effective magnetic moment is 1.81 μ_B and it is almost constant up to 50 K, and then, it starts to decrease and reaches the value of 1.50 μ_B at $T=2$ K. First, the susceptibility was fitted to the Curie–Weiss law (Eq. (1)) and resulted in $g=2.09$ and $\Theta=-0.72$ K. With the aim to utilize also the isothermal magnetization data, the spin Hamiltonian incorporating the Zeeman term and the molecular field correction was used

$$\hat{H} = \mu_B g B \hat{S}_z - zj\langle \hat{S}_z \rangle \hat{S}_z \quad (5)$$

where zj is the common molecular-field parameter, which is due to intermolecular interactions and $\langle \hat{S}_z \rangle$ is a thermal average of the spin projection [23]. Both sets of experimental data were fitted simultaneously and resulted in $g=2.09$ and $zj=-2.37\,\mathrm{cm}^{-1}$ (Fig. 5). Such antiferromagnetic molecular mean-field interactions might be explained by the presence of a variety of non-covalent interactions in the crystal structure of **2** (see Fig. 2).

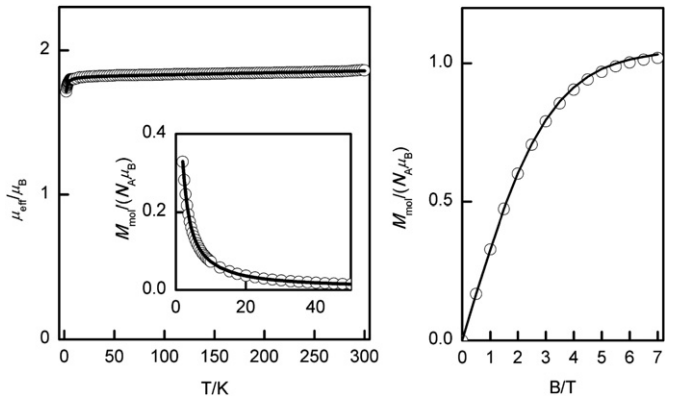

Fig. 4. Magnetic data for **1**. Left: temperature dependence of the effective magnetic moment (calculated from the temperature dependence of magnetization at $B=1$ T). Inset: temperature dependence of the molar magnetization. Right: field dependence of magnetization at $T=2.0$ K. Empty circles: experimental points. Full line: the best fit to the experimental data calculated using Eqs. (3) and (4) with $J=-0.23\,\mathrm{cm}^{-1}$ and $g=2.10$.

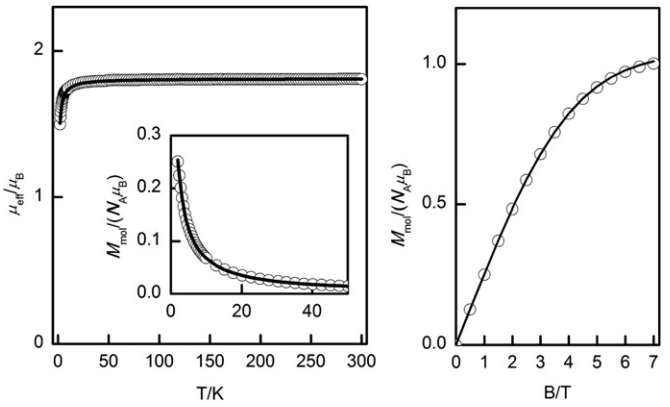

Fig. 5. Magnetic data for **2**. Left: temperature dependence of the effective magnetic moment (calculated from the temperature dependence of magnetization at $B=1$ T). Inset: temperature dependence of molar magnetization. Right: field dependence of magnetization at $T=2.0$ K. Empty circles: experimental points. Full line: the best fit to the experimental data calculated using Eq. (5) with $g=2.09$ and $zj=-2.37\,\mathrm{cm}^{-1}$.

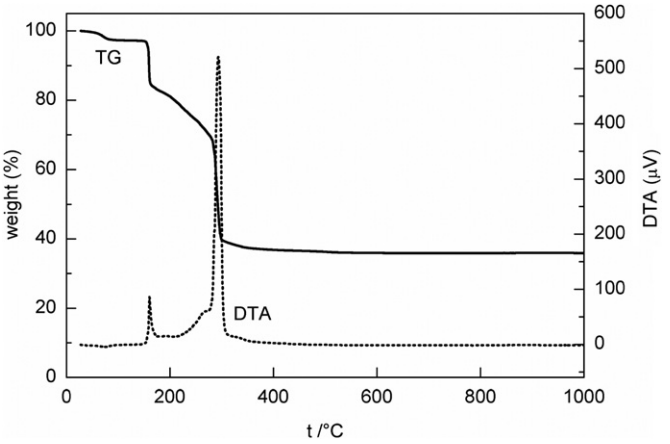

Fig. 6. TG and DTA curves of complex **3**.

3.4. Thermal studies

The thermogravimetric (TG) and differential thermal (DTA) analyses were carried out for all three complexes. The thermal degradation of the compound **3** began at about 30 °C and it may be connected with the partial elimination of the crystal water molecule (weight loss found/calcd. 2.6/4.0%)—Fig. 6. This elimination can be also seen from the DTA curve as an endoeffect with minimum at 74 °C. The existence of an anhydrous complex of **3** was proved within the temperature interval of 95–141 °C. Then, the decay proceeds in a few steps which are accompanied by two sharp exoeffects with the maxima at 161 and 293 °C. The first peak could correspond to the degradation of the *N*-methylethylenediamine molecule attached to the Cu^{II} central atom, and the second peak to the overall decomposition of the complex, which is finished at 568 °C. The degradation product of the complex **3** has been identified as a mixture of $CuFe_2O_4$ and CuO in a molar ratio of 1:1 (proved by X-ray powder diffraction, CuO [01-089-5896] [24], $CuFe_2O_4$ [01-001-9258] [25]—see Fig. A7, in Appendix A, Supplementary Material). The thermal decomposition processes of the complexes **1** and **2** are very similar. In both cases, a mixture

of $CuFe_2O_4$ and CuO was determined as a final product of the conversion.

3.5. Mössbauer spectroscopy

The room temperature ^{57}Fe Mössbauer spectra (see Fig. 7) for compounds **1–3** show well defined doublets with almost the same isomer shift parameters δ (between -0.25 and -0.26 mm/s), which are characteristic for diamagnetic low-spin Fe(III) complexes. The quadrupole splitting parameters ΔE_Q were found to be 0.95 mm/s for **1**, 0.88 mm/s for **2**, and 0.93 mm/s for **3**, and clearly reflect a slightly lower degree of deformation (higher symmetry) in the vicinity of the iron atom in **2** as compared to **1** and **3**. The Mössbauer spectra for compounds **2** and **3** were measured at 25 K and their fitting resulted in $\delta = -0.17\ mms^{-1}$, $\Delta E_Q = 0.89\ mms^{-1}$, and $\delta = -0.16\ mms^{-1}$, $\Delta E_Q = 0.94\ mms^{-1}$, respectively. The changes in the isomer shift values between 300 and 25 K are due to the second-order Doppler effect [26], while the minimum changes in quadrupole splitting indicate a negligible effect of temperature on degree of deformation in the vicinity of iron atoms.

Moreover, the thermal degradation products **2T** and **3T** of the complexes **2**, and **3**, respectively, were also characterized by Mössbauer spectroscopy. The room temperature ^{57}Fe Mössbauer spectra showed the presence of two Fe(III) positions in the spinel structure of $CuFe_2O_4$. The experimental data for **2T** can be successfully described by two sextets with different hyperfine parameters, $\delta_1 = 0.26\ mms^{-1}$, $\Delta E_{Q1} = -0.02\ mms^{-1}$, $B_{hf1} = 48.2$ T and $\delta_2 = 0.36\ mms^{-1}$, $\Delta E_{Q2} = -0.14\ mms^{-1}$, $B_{hf2} = 50.9$ T, with the relative area ratio of $A_1{:}A_2 = 70{:}30$—Fig. 7. The first sextet can be assigned to Fe(III) in tetrahedral (T_d) positions while the second one to Fe(III) in octahedral (O_h) positions within the spinel structure [27]. The **3T** sample exhibited comparable spectral characteristics and the experimental data were simulated using $\delta_1 = 0.27\ mms^{-1}$, $\Delta E_{Q1} = -0.03\ mms^{-1}$, $B_{hf1} = 47.9$ T, and $\delta_2 = 0.37\ mms^{-1}$, $\Delta E_{Q2} = -0.17\ mms^{-1}$, $B_{hf2} = 50.8$ T, with the area ratio of $A_1{:}A_2 = 76{:}24$.

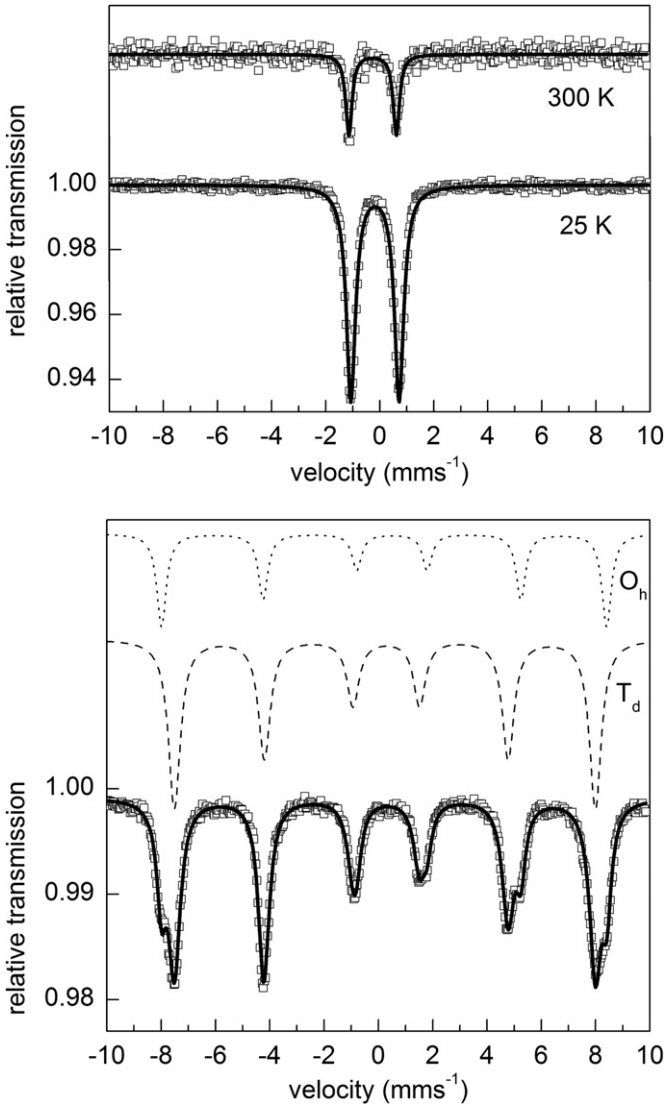

Fig. 7. Top: ^{57}Fe Mössbauer spectra for complex **2** measured at $T = 25$ and 300 K. Bottom: the room temperature ^{57}Fe Mössbauer spectrum of the decomposition product of **2**, including two fitted subspectra corresponding to octahedral (O_h) and tetrahedral (T_d) positions in the $CuFe_2O_4$ structure. The cross symbols represent the experimental data and the lines represent the best fit data.

3.6. Electron microscopy techniques

Scanning electron microscope (SEM) images of the thermal degradation products **2T** and **3T** show the presence of well developed nanocrystals exhibiting the various sizes and morphology—Fig. 8. Nevertheless, the deeper analysis of the particles observed in decomposition products indicate two types of crystals

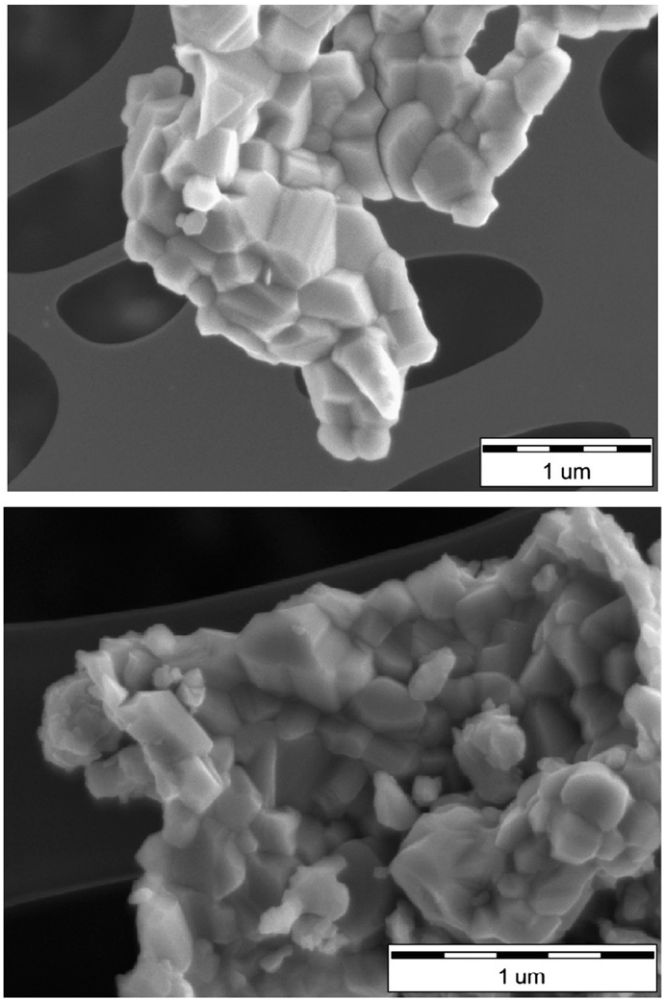

Fig. 8. SEM images of mixtures of $CuFe_2O_4$ and CuO nanoparticles prepared by thermal treatment of **2** (top) and **3** (bottom) as the precursors.

differing in size. The smaller particles ranging between 50 and 150 nm would be assigned to $CuFe_2O_4$, while the bigger ones (250–550 nm) could correspond to CuO, as clearly confirmed by EDS analysis (see Fig. A8; in Appendix A, Supplementary Material).

4. Conclusions

In this work, three bimetallic copper(II)–iron(III) complexes containing the nitroprusside anion were prepared and characterized by a broad spectrum of physical techniques. The X-ray analysis revealed the one-dimensional molecular structure of **1** and **3** and binuclear structure of **2**. The Mössbauer spectroscopy showed that the iron(II) centers are in the low-spin diamagnetic state in the whole temperature interval. The magnetic measurements confirmed the weak antiferromagnetic exchange among the paramagnetic Cu(II) centers in 1D chains of **1** and **3** and quite intense intermolecular interactions of the antiferromagnetic nature in case of compound **2** mainly due to hydrogen bonds. The presented compounds were also tested as potential candidates for the thermal preparation of spinel structure $CuFe_2O_4$ nanoparticles.

5. Supplementary materials

CCDC 753577, 753578 and 753579 contain the supplementary crystallographic data for **1**, **2**, and **3**, respectively. These data can be obtained free of charge via http://www.ccdc.cam.ac.uk/conts/retrieving.html, or from the Cambridge Crystallographic Data Centre, 12 Union Road, Cambridge CB2 1EZ, UK; fax: (+44) 1223 336 033; or e-mail: deposit@ccdc.cam.ac.uk. Figs. A1–A4 contain additional structural and magnetic data of 3, Figs. A5 and A6 and Table A1 support magnetic modeling, Fig. A7 shows XRD data of thermal degradation products of 2 and 3, Fig. A8 shows SEM and EDS patterns of 2.

Acknowledgments

We acknowledge the financial support from the Czech Ministry of Education, Youth and Sports (MSM6198959218) and the Academy of Sciences of the Czech Republic (KAN115600801). We thank Dr. Dalibor Jančík for SEM analyses of the samples.

Appendix A. Supplementary material

Supplementary data associated with this article can be found in the online version at doi:10.1016/j.jssc.2010.03.001.

References

[1] (a) J. Černák, M. Orendáč, I. Potočňák, J. Chomič, A. Orendáčová, J. Skoršepa A. Feher, Coord. Chem. Rev. 224 (2002) 51;
(b) M. Verdaguer, A. Bleuzen, V. Marvaud, J. Vaissermann, M. Seuleiman C. Desplanches, Scuiller, C. Train, R. Garde, G. Gelly, C. Lomenech I. Rosenman, P. Veillet, C. Cartier, F. Villain, Coord. Chem. Rev. 192 (1999) 1023 and references cited therein.
[2] (a) Y. Sadaoka, H. Aono, E. Traversa, M. Sakamoto, J. Alloys Compd. 278 (1998) 135;
(b) R. Brahmi, C. Kappenstein, J. Černák, D. Duprez, in: B. Delmon et al.(Ed.), Preparation of Catalysts, Elsevier, Amsterdam, 1998, p. 403.
[3] (a) U. Hauser, V. Oestreich, H.D. Rohrweck, Z. Phys. 17 (1977) A280;
(b) Th. Woike, W. Krasser, P.S. Bechthold, S. Haussühl, Phys. Rev. Lett. 53 (1984) 1767;
(c) M.D. Carducci, D.V. Fomitchev, P. Coppens, J. Am. Chem. Soc. 119 (1997) 2669;
(d) F. Bellouard, M. Clemente-León, E. Coronado, J.R. Galán-Mascarós, C. Giménez-Saiz, C.J. Goméz- García, Th. Woike, Polyhedron 20 (2001) 1615.
[4] F.H. Allen, Acta Cryst. B 58 (2002) 380.
[5] (a) K.L. Zhang, Y. Xu, Z. Wang, C.M. Jin, X.Z. You, Transition Met. Chem. 27 (2002) 95;
(b) J.H. Zou, X.Y. Xu, Z. Xu, X.Z. You, X.Y. Huang, W.L. Zhang, X.P. Shen, Y.P. Yu, J. Coord. Chem. 43 (1998) 273;
(c) X. Peng, H.Z. Kou, M. Xiong, R.J. Wang, Acta Cryst. E 59 (2003) 252;
(d) L.X. Yang, W.B. Wang, S. Xia, S.Y. Wu, J. Coord. Chem. 61 (2008) 2549;
(e) L. Shen, Y.J. Zhang, G.D. Sheng, H.T. Wang, Acta Cryst. C 58 (2002) 382;
(f) S.W. Liang, M.X. Li, M. Shao, H.J. Liu, J. Mol. Struct. 841 (2007) 73;
(g) M. Mondal, M.K. Saha, S. Mitra, V. Gramlich, M.S. El Fallad, Polyhedron 19 (2000) 1935;
(h) Z. Smékal, Z. Trávníček, J. Marek, M. Nádvorník, Aust. J. Chem. 53 (2000) 225;
(i) H.L. Shyu, H.H. Wei, J. Coord. Chem. 47 (1999) 319.
[6] B.C. Zhou, H.Z. Kou, Y. Li, M. Xiong, R.J. Wang, Chin. J. Chem. 21 (2003) 1159.
[7] (a) Y.S. You, J.H. Yoon, J.H. Lim, H.C. Kim, C.S. Hong, Inorg. Chem. Acta 360 (2007) 2523;
(b) Z. Smékal, J. Kameníček, I. Svoboda, A. Escuer, Collect. Czech. Chem. Commun. 66 (2001) 1490;
(c) H.Z. Kou, H.M. Wang, D.Z. Liao, P. Cheng, Z.H. Jiang, S.P. Yan, X.Y. Huang, G.L. Wang, Aust. J. Chem. 51 (1998) 661;
(d) H.Z. Kou, H.M. Wang, D.Z. Liao, P. Cheng, Z.H. Jiang, S.P. Yan, X.Y. Huang, G.L. Wang, Aust. J. Chem. 51 (1998) 661;
(e) C.Q. Liu, J.M. Shi, W. Xu, Y.Q. Chen, Pol. J. Chem. 77 (2003) 929.
[8] Z.N. Chen, J.L. Wang, J. Qiu, F.M. Miao, W.X. Tang, Inorg. Chem. 34 (1995) 2255.
[9] D.F. Mullica, D.B. Tippin, E.L. Sappenfield, J. Coord. Chem. 25 (1992) 175.
[10] (a) A.J. Baden-Fuller, Ferrites at Microwave Frequencies, Institution of Engineering and Technology, Peter Peregrinus Ltd, London, 1987;
(b) T. Moulson, J. Herbert, Electroceramics: Materials, Properties, Application, Springer, 1990;
(c) A. Goldman, Handbook of Ferromagnetic Materials and Applications, 2nd Edition, Kluwer, Norwell, 2002;
(d) A. Goldman, Modern Ferrite technology, 2nd Edition, Springer, New York, 2006.
[11] Y. Teraoka, W.F. Shangguan, S. Kagawa, Res. Chem. Intermed. 26 (2000) 201.
[12] (a) N. Shimoda, K. Faungnawakij, R. Kikuchi, T. Fukunaga, K. Eguchi, Appl. Catal. A—Gen. 365 (2009) 71;
(b) K. Faungnawakij, N. Shimoda, T. Fukunaga, R. Kikuchi, K. Eguchi, Appl. Catal. B—Environ. 92 (2009) 341–350.
[13] (a) M. Brezeanu, E. Segal, C. Eugen, A. Contescu, L. Patron, Rev. Chim.—Bucharest 40 (1989) 510;
(b) G. Marinescu, L. Patron, O. Carp, L. Diamandescu, N. Stanica, A. Meghea, M. Brezeanu, J.C. de Greniere, J. Etourneaue, J. Mater. Chem. 12 (2002) 3458;
(c) D. Gingasu, L. Patron, I. Mindru, N. Stanica, I. Balint, Rev. Roum. Chim. 49 (2004) 669;
(d) D. Gingasu, I. Mindru, O. Carp, L. Patron, S. Stoleriu, Rev. Roum. Chim. 51 (2006) 795;
(e) O. Carp, D. Gingasu, I. Mindru, L. Patron, Thermochim. Acta 449 (2006) 55;
(f) D. Gingasu, I. Mındru, L. Patron, O. Carp, D. Matei, C. Neagoe, I. Balint, J. Alloys Compd. 425 (2006) 357.
[14] M.P. Suh, S.G. Kang, T.M. Chung, Bull. Korea Chem. Soc. 11 (1990) 206.
[15] E. König, Magnetic Properties of Coordination and Organometallic Transition Metal Compounds, Springer-Verlag, Berlin, 1966.
[16] CrysAlis RED and CrysAlis CCD, Version 1.171.32.11, Oxford Diffraction Ltd., Abingdon, England, 2006.
[17] G.M. Sheldrick, Acta Cryst. A 64 (2008) 112.
[18] Diamond – crystal and molecular structure visualization, crystal impact —K. Brandenburg & H. Putz GbR, Postfach 1251, D-53002 Bonn.
[19] (a) K. Nakamoto, Infrared and Raman Spectra of Inorganic and Coordination Compounds, Part B, 5th edn., Wiley, New York, 1997;
(b) S. Zhan, X. Chen, A. Vij, D. Guo, Q. Meng, Inorg. Chim. Acta 292 (1999) 157.
[20] G. Wilkinson, R.D. Gillard, J.A. McCleverty, Comprehensive Coordination Chemistry, Vol. 4, Pergamon Press, 1987.
[21] R. Boča, Struct. Bond. 117 (2006) 172.
[22] D.C. Johnston, R.K. Kremer, M. Troyer, X. Wang, A. Klümper, S.L. Budko, A.F. Panchula, P.C. Canfield, Phys. Rev. B 61 (2000) 9558.
[23] R. Boča, Theoretical Foundations of Molecular Magnetism, Elsevier, Amsterdam, 1999.
[24] (a) ICDD powder diffraction database file card number [01-089-5896].;
(b) V. Massarotti, D. Capsoni, M. Bini, A. Altomare, A.G.G. Moliterni, Z. Kristallogr. 213 (1998) 259.
[25] (a) ICDD powder diffraction database file card number [01-001-9258];
(b) M.A. Zinovik, A.A. Shchepetkin, G.I. Chufarov, Inorg. Mater. (Engl. Transl.) 7 (1971) 119.
[26] N.N. Greenwood, T.C. Gibb, in: Mössbauer Spectroscopy, Chapman and Hall Ltd, London, 1971.
[27] G.F. Goya, H.R. Rechenberg, Nanostructured Mater. 10 (1998) 1001.